
Article:
Xu, H., Xiao, S., Li, Z. et al. (3 more authors) (2022) A novel SAR imaging method based on morphological component analysis. IEEE Sensors Journal, 22 (13). pp. 13326-13337. ISSN 1530-437X

https://doi.org/10.1109/jsen.2022.3179607

A Novel SAR Imaging Method Based on Morphological Component Analysis

Huaping Xu, *Member*, *IEEE,* Shuangying Xiao, Zhaohong Li, Shuang Wang, Wei Liu, *Member, IEEE,* and Jingwen Li

***Abstract*—Clutter suppression plays an important role in a synthetic aperture radar (SAR) system. The conventional SAR imaging methods are useful for distinguishing the echo signal and noise, but cannot separate the target signal from background clutter. Inspired by the signal separation ability of morphological component analysis (MCA), a novel SAR imaging method based on MCA is proposed to suppress the strong background clutter. In the new model, the SAR echo is considered as a linear superposition of target signal, clutter signal, and noise. According to different characteristics of morphological components, clutter dictionary and target dictionary are constructed to sparsely represent the clutter component and target component, respectively. Then, the MCA method based on the sparse representation and morphological diversity of signals is employed to decompose the SAR echo into the target signal, clutter signal, and noise. Finally, the separated target signal is processed to obtain the ultimate SAR image. Experimental results from simulated and real SAR data are provided to demonstrate the effectiveness of the proposed method.**

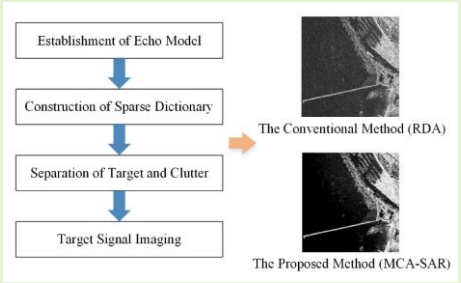

***Index Terms*—SAR imaging, Clutter suppression, Morphological component analysis.**

I. Introduction

SYNTHETIC aperture radar (SAR) has been widely used in defense and civilian applications [1]. It actively transmits electromagnetic waves to the observed scene, receives its scattering echo and performs SAR imaging to obtain the corresponding images.

In addition to the target signal, the SAR echo also includes clutter signal and noise. Any signal other than the scattering echo reflected from the observed scene is considered as noise, such as the thermal noise generated by the radar system [2]. Clutter signal is a concept relative to the target signal of interest [3], which can be defined as the echo signal in a scene that the observer is not interested in [4], such as echo generated by land, ocean, and other backgrounds. In the applications of SAR images, noise and clutter will affect the imaging performance, and especially strong clutter will mask weak targets, and affect the following target detection, classification, and recognition results [5]. Since the conventional SAR imaging methods apply the same processing to the clutter signal and target signal, they are enhanced simultaneously by the algorithm and it may become difficult to separate clutter and target in the resultant SAR image; as a result, the weak target may be degraded when suppressing the clutter directly in the SAR image domain. One possible solution to this problem is to perform clutter suppression in the imaging process before obtaining the final SAR images.

The existing SAR imaging methods can be classified into two types: matched filtering based and parameter estimation based. The first type includes the back-projection (BP) algorithm [6], the range-Doppler algorithm (RDA) [7], the chirp-scaling algorithm (CSA) [8], and the Omega-K algorithm (ωKA) [9], etc. The BP algorithm obtains the SAR image by range compression, spatial domain interpolation, and azimuth coherent addition [10]. The other algorithms, known as the frequency-domain approach, usually consist of the following main operations: range compression, range migration correction, and azimuth compression. Different implementations of range migration correction distinguish these different imaging algorithms. Matched filtering is applied in range compression and azimuth compression [11], and it is derived from the maximum signal-to-noise ratio (SNR) criterion. When SAR echo passes through a suitable matched filter, the signal, including target signal and clutter signal, is concentrated to the peak, and the noise is suppressed.

Spectrum estimation [12] and compressed sensing (CS) based SAR imaging [13] are representatives of the second type. A well-known example for spectrum estimation is the multiple signal classification (MUSIC) algorithm [14], which decomposes the covariance matrix of the measurement data into signal subspace and noise subspace. Orthogonality of the two subspaces is used to construct the spatial spectrum function, and the signal can be detected from the MUSIC spectrum by peak

Manuscript received XXX, 2021; revised XXX, 2022; accepted XXX, 2022.

Huaping Xu is with the School of Electronic and Information Engineering, Beihang University, 37 Xueyuan Road, Beijing,100191, P.R. China (phone: 86-10-82338154; fax: 86-10-82338154; e-mail: xuhuaping@buaa.edu.cn).

Wei Liu is with the Department of Electronic and Electrical Engineering, University of Sheffield, Mappin Street, Sheffield S1 3JD, UK (e-mail: w.liu@sheffield.ac.uk).

Shuangying Xiao, Zhaohong Li, Shuang Wang, and Jingwen Li are with the School of Electronic and Information Engineering, Beihang University, 37 Xueyuan Road, Beijing, 100191, P.R. China.

search while noise is suppressed. The CS-based SAR imaging (CS-SAR) method can reconstruct the signal with less measurement data than that required by the Nyquist sampling theorem, which solves the problem of high data rate caused by increasing resolution and swath [15] [16]. In [17], a one-dimensional CS-SAR method was proposed, which applies the CS method to the azimuth data after range compression. A feasible CS-SAR method from the raw data domain was proposed in [18], which uses the geometric relationship between radar platform and observed scene to construct the observation matrix and exactly recover the scattered field to obtain the SAR image. A fast CS-SAR method was introduced in [19] by taking the inverse of focusing procedures as the observation matrix. To achieve noise suppression and reconstruct the signal, these CS-SAR methods use the difference in sparse characteristics between the signal and noise, i.e., both the target signal and clutter signal can be reconstructed according to the observation matrix, whereas the noise cannot.

As can be seen, both types of SAR imaging algorithms work by dividing the echo into two parts, signal and noise, and then suppressing noise in the imaging process. Since the clutter signal is modeled as part of the signal, these imaging algorithms perform the same processing on clutter signal and target signal, and as a result, cannot suppress the background clutter during imaging. Therefore, it may be beneficial to find a new imaging method that can suppress clutter in the imaging process.

Morphological component analysis (MCA) is a signal separation method based on sparse representation, which has been extensively applied in the image domain. The work in [20] and [21], although not involving the imaging process, shows the ability of MCA to separate target and clutter in ultrasound and radar images. Motivated by the advantages of MCA in signal decomposition, in this work, MCA is introduced in the SAR echo domain, and a novel SAR imaging method is proposed, which suppresses clutter signal and noise and improves imaging quality by extracting the target signal from SAR echo during imaging, denoted as MCA-SAR. First, a new SAR echo model is established, which divides the SAR echo into three parts: target signal, clutter signal, and noise. Then, the target dictionary and clutter dictionary are constructed, and the MCA method is used to separate the three components. Finally, the separated target signal is processed in a normal way by existing imaging algorithms. It is shown by experimental results that the proposed MCA-SAR method can effectively suppress noise and clutter while keeping the target information.

The remainder of this paper is organized as follows. In Section II, the fundamentals of the CS-SAR and MCA are introduced. The proposed MCA-SAR method is presented in Section III. In Section IV, results based on simulated and real SAR echo data are provided, and Section V concludes the paper.

II. CS-based SAR Imaging And Morphological Component Analysis

A. CS-based SAR Imaging

In SAR imaging, the received echo $s(\tau, a)$ can be considered as the convolution of the transmitted pulse $h(\tau, a)$ of SAR and the scene reflectivity function $\sigma(\tau, a)$, corrupted by the noise $n(\tau, a)$ [7]:

$$s(\tau, a) = h(\tau, a) * \sigma(\tau, a) + n(\tau, a) \tag{1}$$

where τ and a are range time and azimuth time, respectively. The convolution operation can be represented in a general matrix form as:

$$\mathbf{s} = \mathbf{H}\boldsymbol{\sigma} + \mathbf{n} \tag{2}$$

where $\mathbf{s} = \mathrm{vec}(\mathbf{S}) \in C^{M\times 1}$, $\mathbf{S} \in C^{N_a \times N_r}$ is SAR echo, $M = N_a \times N_r$, $\mathrm{vec}(\cdot)$ stands for matrix vectorization, N_r and N_a are the range and azimuth sampling number, respectively. $\boldsymbol{\sigma} \in C^{N\times 1}$ is the scattering coefficient vector of the observed scene, N denotes the number of coefficients, and $\mathbf{n} \in C^{M\times 1}$ is the additive noise vector. $\mathbf{H} \in C^{M\times N}$ is the observation matrix.

In the CS-SAR model [22], the echo data $\mathbf{s}$ is sampled and compressed with a random down-sampling matrix $\boldsymbol{\Theta} \in C^{F\times M}$, $F \ll N$, and (2) can be rewritten as:

$$\mathbf{s}_s = \boldsymbol{\Theta}\mathbf{H}\boldsymbol{\sigma} + \mathbf{n} \tag{3}$$

where $\mathbf{s}_s$ is down-sampled echo datum. When $\boldsymbol{\sigma}$ is sparse enough, i.e., most of the entries are zeros, and the sensing matrix $\boldsymbol{\Psi} = \boldsymbol{\Theta}\mathbf{H}$ satisfies some conditions such as restricted isometry property (RIP) [23], $\boldsymbol{\sigma}$ can be exactly recovered from the ill-posed linear system $\mathbf{s}_s = \boldsymbol{\Psi}\boldsymbol{\sigma} + \mathbf{n}$. In detail, $\boldsymbol{\sigma}$ can be reconstructed by the following constrained L_1 norm minimization problem:

$$\boldsymbol{\sigma} = \arg\min_{\boldsymbol{\sigma}} \|\boldsymbol{\sigma}\|_1 \quad \text{s.t.} \quad \mathbf{s}_s = \boldsymbol{\Psi}\boldsymbol{\sigma} \tag{4}$$

There are several algorithms available to solve (4), such as the matching pursuit (MP) [24], the iterative thresholding algorithm (ITA) [25], and the orthogonal matching pursuit (OMP) [26] techniques.

Since SAR imaging can be regarded as a linear process, the scattering coefficient $\boldsymbol{\sigma}$ can be recovered by the echo $\mathbf{s}_s$ and the sensing matrix $\boldsymbol{\Psi}$.

B. Morphological Component Analysis

MCA is a signal decomposition method based on sparse representation, which uses different dictionaries to decompose the signal into different components containing different types of information [27].

The MCA method assumes the signal $\mathbf{Y}$ is a linear superposition of W morphological components:

$$\mathbf{Y} = \mathbf{y}_1 + \mathbf{y}_2 + \cdots + \mathbf{y}_i + \cdots + \mathbf{y}_W \tag{5}$$

where $\mathbf{y}_i$ is the ith morphological component of the signal $\mathbf{Y}$. Assuming that each component $\mathbf{y}_i$ can be sparsely represented by dictionary $\boldsymbol{\Phi}_i$, $\mathbf{y}_i$ can be rewritten as:

$$\mathbf{y}_i = \boldsymbol{\Phi}_i\boldsymbol{\alpha}_i \quad i = 1,2,\cdots,W \tag{6}$$

where $\boldsymbol{\alpha}_i$ is the sparse coefficient vector. To successfully separate signal $\mathbf{Y}$ into different components, $\mathbf{y}_i$ can only be sparsely represented by dictionary $\boldsymbol{\Phi}_i$ but not other dictionaries $\boldsymbol{\Phi}_l, l \neq i$. The dictionary $\boldsymbol{\Phi}_i$ plays an important role in the separation and discrimination between different morphological component signals.

Based on the above assumptions, the sparse representation of the signal $\mathbf{Y}$ can be obtained by solving the following optimization problem:

$$\{\boldsymbol{\alpha}_1 \ \cdots \ \boldsymbol{\alpha}_W\} = \arg\min_{\{\boldsymbol{\alpha}_1 \cdots \boldsymbol{\alpha}_W\}} \sum_{i=1}^{W} \|\boldsymbol{\alpha}_i\|_0 \quad \text{s.t.} \quad \mathbf{Y} = \sum_{i=1}^{W} \boldsymbol{\Phi}_i\boldsymbol{\alpha}_i \tag{7}$$

By basis pursuit (BP) [28], (7) is usually converted to the following form by replacing the L_0 norm with the L_1 norm.

$$\{\boldsymbol{\alpha}_1 \ \cdots \ \boldsymbol{\alpha}_W\} = \arg \min_{\{\boldsymbol{\alpha}_1 \ \cdots \ \boldsymbol{\alpha}_W\}} \sum_{i=1}^{W} \|\boldsymbol{\alpha}_i\|_1 + \beta \left\| \mathbf{Y} - \sum_{i=1}^{W} \boldsymbol{\Phi}_i \boldsymbol{\alpha}_i \right\|_2^2 \quad (8)$$

In (8), β is the regularization parameter. Each component of the signal can be reconstructed according to the sparse coefficients and the corresponding dictionary.

III. SAR Imaging Method Based on MCA

In this section, a novel SAR imaging method based on MCA is proposed, followed by details of its implementation.

A. The Proposed MCA-SAR Imaging Method

First, a new echo model is established by dividing the SAR echo into three parts: target signal, clutter signal, and noise; then, the sparse dictionaries for target scattering coefficient and clutter scattering coefficient are respectively constructed with their individual characteristics; by applying the MCA method the three components are recovered from the SAR echo; finally, only the target signal component is processed for imaging to achieve noise and clutter suppression.

1) The New Echo Model: Traditionally, the SAR echo is considered as the superposition of signal and noise. Since the clutter signal and target signal are treated in the same way, the clutter signal is enhanced together with the target signal during the imaging process, making it difficult to suppress the clutter in the SAR image. In this work, the SAR echo is decomposed into three components: target signal $\mathbf{T}$, clutter signal $\mathbf{C}$, and noise $\mathbf{n}$, as follows:

$$\mathbf{s} = \mathbf{T} + \mathbf{C} + \mathbf{n} = \mathbf{H}(\mathbf{t} + \mathbf{c}) + \mathbf{n} \quad (9)$$

where $\mathbf{t}$ and $\mathbf{c}$ are the scattering coefficient of the target and clutter, respectively. When the spatial distribution of the scattering coefficient of the observed scene is sparse, the scene can be directly restored according to the observation matrix $\mathbf{H}$. However, for scenes with complex spatial distribution of scattering coefficient, it is necessary to find a dictionary that can sparsely represent a morphological component and only this component is recovered through the corresponding sparse reconstruction process. With dictionary $\boldsymbol{\Phi}_t$ for sparse representation of $\mathbf{t}$ and $\boldsymbol{\Phi}_c$ for sparse representation of $\mathbf{c}$, (9) can be rewritten as:

$$\mathbf{s} = \mathbf{H}(\boldsymbol{\Phi}_t \boldsymbol{\alpha}_t + \boldsymbol{\Phi}_c \boldsymbol{\alpha}_c) + \mathbf{n} = \mathbf{A}_t \boldsymbol{\alpha}_t + \mathbf{A}_c \boldsymbol{\alpha}_c + \mathbf{n} \quad (10)$$

where $\boldsymbol{\alpha}_t$ and $\boldsymbol{\alpha}_c$ are the sparse coefficients of $\mathbf{t}$ and $\mathbf{c}$ in the dictionary $\boldsymbol{\Phi}_t$ and $\boldsymbol{\Phi}_c$, respectively. In (10), $\mathbf{A}_t = \mathbf{H}\boldsymbol{\Phi}_t$, $\mathbf{A}_c = \mathbf{H}\boldsymbol{\Phi}_c$, the observation matrix $\mathbf{H}$ is defined in the same way as that in CS-SAR, and please refer to [17], [19] for its construction in detail.

In practice, when $\mathbf{t}$ is sparse in the spatial domain, the target dictionary $\boldsymbol{\Phi}_t$ can be replaced by the identity matrix I, and (10) becomes:

$$\mathbf{s} = \mathbf{H}(I\boldsymbol{\alpha}_t + \boldsymbol{\Phi}_c \boldsymbol{\alpha}_c) + \mathbf{n} = \mathbf{H}\boldsymbol{\alpha}_t + \mathbf{A}_c \boldsymbol{\alpha}_c + \mathbf{n} \quad (11)$$

2) Construction of Dictionaries: An appropriate dictionary can increase the sparseness of coefficients and improve the accuracy of sparse reconstruction. Therefore, construction of the dictionary is very important for the MCA-SAR method. It can take two main forms, fixed dictionary and learned dictionary. The fixed one is based on specific mathematical transformations, such as wavelets [29], curvelets [30], and discrete cosine transform (DCT) [31]. These fixed dictionaries have a simple structure and low complexity, but poor adaptability to complex scenes.

The learned dictionary is constructed by the dictionary learning method and training data, whose atoms can directly capture features of the signals. The purpose of dictionary learning methods is to create a learned dictionary that provides the sparsest reconstruction for the training data [32]. Dictionary learning methods have been widely used in SAR signal processing, including the algorithm of optimal directions (MOD) [33], the online dictionary learning (ODL) algorithm [34], and the K-singular value decomposition (K-SVD) algorithm [35]. These learned dictionaries have strong adaptability, but with relatively high computational complexity.

Since different dictionaries can represent different local features or global information, a well-chosen dictionary can lead to a sparse representation of the target or clutter and highlight their corresponding features.

3) Separation of Target and Clutter: MCA has been successful in decomposing signal into distinct components [36] [37]. After obtaining the target dictionary $\boldsymbol{\Phi}_t$ and clutter dictionary $\boldsymbol{\Phi}_c$, the target and clutter components can be separated by MCA. The sparse coefficients $\boldsymbol{\alpha}_t$ and $\boldsymbol{\alpha}_c$ in (10) can be solved by (8) as:

$$\{\boldsymbol{\alpha}_t, \boldsymbol{\alpha}_c\} = \arg \min_{\{\boldsymbol{\alpha}_t, \boldsymbol{\alpha}_c\}} \|\boldsymbol{\alpha}_t\|_1 + \|\boldsymbol{\alpha}_c\|_1 + \beta \|\mathbf{s} - \mathbf{A}_t \boldsymbol{\alpha}_t - \mathbf{A}_c \boldsymbol{\alpha}_c\|_2^2 \quad (12)$$

The sparse coefficients $\boldsymbol{\alpha}_t$ and $\boldsymbol{\alpha}_c$ can be converted into the target component $\mathbf{T}$ and clutter component $\mathbf{C}$. The obtained optimization problem becomes:

$$\{\mathbf{T}, \mathbf{C}\} = \arg \min_{\{\mathbf{T},\mathbf{C}\}} \|\mathbf{A}_t^+ \mathbf{T}\|_1 + \|\mathbf{A}_c^+ \mathbf{C}\|_1 + \beta \|\mathbf{s} - \mathbf{T} - \mathbf{C}\|_2^2 \quad (13)$$

where $\mathbf{A}_t^+$ and $\mathbf{A}_c^+$ are the pseudoinverse of $\mathbf{A}_t$ and $\mathbf{A}_c$, respectively. The separation of the target signal and clutter signal based on MCA can be achieved by solving (13).

4) Target Signal Imaging: After recovering the target signal from the SAR echo, existing imaging algorithms can be employed to form the SAR image of the target:

$$\mathbf{I}_t = \mathrm{M}(\mathbf{T}_{2\mathrm{D}}) \quad (14)$$

where $\mathrm{M}(\cdot)$ represents the SAR imaging process, $\mathbf{T}_{2\mathrm{D}}$ is the two-dimensional target signal, whose vector form is the signal component $\mathbf{T}$, with $\mathbf{T} = \mathrm{vec}(\mathbf{T}_{2\mathrm{D}})$, and $\mathbf{I}_t$ is the SAR imaging result. Due to linearity of most imaging algorithms, $\mathrm{M}(\cdot)$ can be written in the form of a matrix $\mathbf{M}$. Equation (14) can be expressed as:

$$\tilde{\mathbf{t}} = \mathbf{M}\mathbf{T} \quad (15)$$

So, $\tilde{\mathbf{t}} = \mathrm{vec}(\mathbf{I}_t)$ can be regarded as the reconstruction of scattering coefficient $\mathbf{t}$.

B. Implementation of MCA-SAR

The implementation procedure for the proposed MCA-SAR method is shown in Fig. 1. The main processing steps include observation matrix construction, dictionary construction, SAR echo sparse decomposition, and target signal imaging. The observation matrix can be constructed by referring to the CS-SAR method; the curvelet dictionary and the DCT dictionary

are used to construct the target dictionary and the initial clutter dictionary, respectively; the MCA method is used to recover the continue the update of the clutter dictionary using the K-SVD algorithm.

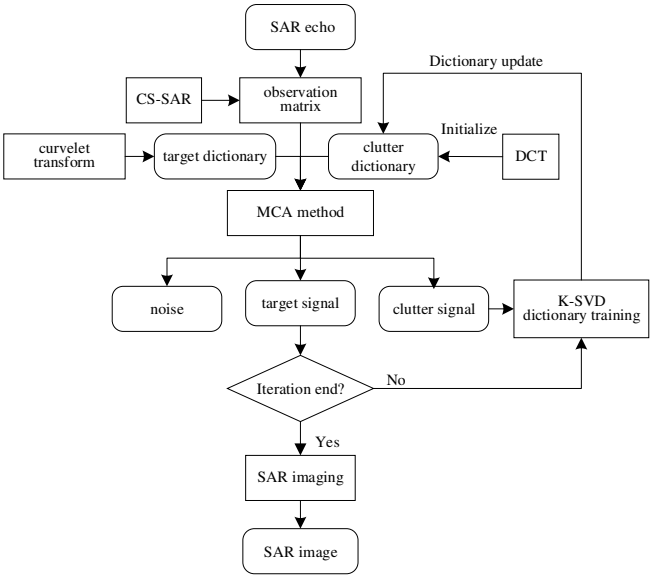

Fig. 1. Flowchart of the proposed MCA-SAR method.

1) Constructing the Observation Matrix: According to (10), a suitable observation matrix $\mathbf{H}$ needs to be constructed first. Due to high computational cost of the time-domain construction method, an approximate observation method in fast CS-SAR [19] is used here. It considers the well-focused image as an estimation of the true scattering coefficient. $\mathbf{H}$ can be approximated as the simulation operator $\mathbf{U}$ which is the inverse imaging process. So,

$$\mathbf{H} \approx \mathbf{U} \tag{16}$$

The RDA is a basic and popular imaging algorithm used in SAR data processing. Taking it as an example, the imaging function $\mathrm{M}(\cdot)$, operated on the two-dimensional array, can be expressed as

$$\mathbf{I} = \mathrm{M}(\mathbf{S}) = \mathbf{F}_a^H\{\mathbf{P}_a \circ \mathbb{C}\langle \mathbf{F}_a[\mathbf{P}_\tau \circ (\mathbf{S}\mathbf{F}_\tau)]\mathbf{F}_\tau^H\rangle\} \tag{17}$$

where $\mathbf{I}$ is SAR image, $\circ$ represents the Hadamard product, $\mathbf{F}_a$ and $\mathbf{F}_\tau$ represent the discrete Fourier transform (DFT) matrix of the azimuth and range direction respectively, $\mathbf{F}_a^H$ and $\mathbf{F}_\tau^H$ represent the inverse DFT matrix of the azimuth and range direction respectively, $\mathbb{C}\langle\cdot\rangle$ is the range cell migration correction (RCMC) interpolation operator, and $\mathbf{P}_a$ and $\mathbf{P}_\tau$ are respectively the matched filter matrices in the azimuth and range direction.

The inverse imaging procedure $\mathrm{U}(\cdot)$ of the RDA can be expressed as:

$$\mathbf{S} = \mathrm{U}(\mathbf{I}) = \{\mathbf{P}_\tau^* \circ [\mathbf{F}_a^H \mathbb{C}^{-1}\langle \mathbf{P}_a^* \circ (\mathbf{F}_a\mathbf{I})\rangle]\mathbf{F}_\tau\}\mathbf{F}_\tau^H \tag{18}$$

where $\mathbf{P}_a^*$, $\mathbf{P}_\tau^*$ are conjugates of $\mathbf{P}_a$ and $\mathbf{P}_\tau$, respectively, and $\mathbb{C}^{-1}\langle\cdot\rangle$ is the inverse process of RCMC. Both $\mathrm{M}(\cdot)$ and $\mathrm{U}(\cdot)$ are linear operators, which can also be transformed into a matrix form. More specifically, $\mathbf{M}$ and $\mathbf{U}$ can be described as:

$$\mathbf{M} = \hat{\mathbf{F}}_a^H \hat{\mathbf{P}}_a \hat{\mathbf{Q}} \hat{\mathbf{F}}_a \hat{\mathbf{F}}_\tau^H \hat{\mathbf{P}}_\tau \hat{\mathbf{F}}_\tau \tag{19}$$

$$\mathbf{U} = \hat{\mathbf{F}}_\tau^H \hat{\mathbf{P}}_\tau^* \hat{\mathbf{F}}_\tau \hat{\mathbf{F}}_a^H \hat{\mathbf{B}} \hat{\mathbf{P}}_a^* \hat{\mathbf{F}}_a \tag{20}$$

where

$$\hat{\mathbf{F}}_a = I_{N_r} \otimes \mathbf{F}_a, \hat{\mathbf{F}}_\tau = \mathbf{F}_\tau^T \otimes I_{N_a} \tag{21}$$

target signal and clutter signal from the SAR echo; finally, according to the stop criterion, determine whether or not to

$$\hat{\mathbf{P}}_a = diag\big(\mathrm{vec}(\mathbf{P}_a)\big), \hat{\mathbf{P}}_\tau = diag\big(\mathrm{vec}(\mathbf{P}_\tau)\big) \tag{22}$$

$\hat{\mathbf{B}}$ and $\hat{\mathbf{Q}}$ are the matrix forms of RCMC operator and inverse RCMC operator, respectively.

2) Dictionary Construction: In practice, due to complexity of the observed scene, the clutter may be non-sparse in the spatial domain, so it is necessary to construct a corresponding dictionary in which the clutter becomes sparse. Different dictionaries have different sparse representation competencies for clutter. The better the sparsity of the clutter under the dictionary, the better the clutter reconstruction quality, and the more conducive to clutter separation. Considering variation of the background clutter, the fixed dictionary approach is not suitable for constructing the clutter dictionary, so the dictionary learning method is employed to find the clutter dictionary adaptively.

The MOD and K-SVD are two well-known dictionary learning methods [38]. Their main difference is that the MOD updates the dictionary by global least squares fit, while the K-SVD relies on singular value decomposition [39]. Compared with the MOD, the K-SVD has higher computational efficiency, so it is used in our work to create the clutter dictionary.

The K-SVD algorithm strives to minimize the signal reconstruction error by decomposing the error terms in the iteration process, which solves the following optimization problem [40]:

$$\langle \mathbf{Z}, \mathbf{X}\rangle = \arg\min_{\mathbf{Z},\mathbf{X}}\{\|\mathbf{Z} - \mathbf{D}\mathbf{X}\|_F^2\} = \min_{\mathbf{Z},\mathbf{X}} \sum_{i=1}^{L}\{\|\mathbf{z}_i - \mathbf{D}\mathbf{x}_i\|_F^2\}$$
$$\text{s.t.} \quad \forall i, \|\mathbf{x}_i\|_0 \le T_0 \tag{23}$$

where $\mathbf{Z} = \{\mathbf{z}_i\}_{i=1}^L$ denotes a set of training signals, each column $\mathbf{z}_i$ is a sample of data $\mathbf{Z}$, $\mathbf{D} = \{\mathbf{d}_j\}_{j=1}^K$ is the over-complete dictionary, K is the number of dictionary atom $\mathbf{d}_j$, and $\mathbf{X} = \{\mathbf{x}_i\}_{i=1}^L$ is the sparse coefficients. T_0 is the sparsity constraint, ensuring that each sparse representation coefficient vector $\mathbf{x}_i$ contains no more than T_0 non-zero entries.

The K-SVD dictionary training algorithm can be divided into two stages: sparse coding and dictionary-update. Table I details the process.

TABLE I
THE K-SVD ALGORITHM

Initialization: the training signals $\mathbf{Z}$, the initial dictionary $\mathbf{D}_0$, and the number of dictionary atoms K. Set $J = 1$.
Loop: Repeat until convergence
1. Sparse Coding Stage: Set $\mathbf{D}_{(J-1)}$ fixed to compute the corresponding sparse coefficients $\mathbf{X}$ of training signals $\mathbf{Z} = \{\mathbf{z}_i\}_{i=1}^L$, by solving:
$$\mathbf{X}_{(J)} = \arg\min_{\mathbf{X}}\left\{\left\|\mathbf{Z} - \mathbf{D}_{(J-1)}\mathbf{X}\right\|_F^2\right\} \quad \text{s.t.} \quad \forall i, \|\mathbf{x}_i\|_0 \le T_0$$
2. Dictionary-Update Stage: update each dictionary atom.
For $k = 1$ to K
(1) Define the group of example signals: $\omega_k = \{i | 1 \le i \le L, \mathbf{X}_{(J)}[k,i] \ne 0\}$
(2) Compute the error matrix: $\mathbf{E}_k = \mathbf{Z} - \sum_{j \ne k} \mathbf{d}_j \mathbf{x}_T^j$,where $\mathbf{x}_T^j$ is the jth rows of matrix $\mathbf{X}_{(J)}$.
(4) Acquire $\mathbf{E}_k^R$ by selecting the column of $\mathbf{E}_k$ that only corresponds to ω_k. Decompose the restricted matrix $\mathbf{E}_k^R$ with SVD: $\mathbf{E}_k^R = \mathbf{G}\Delta\mathbf{V}^T$
(5) Update the dictionary atom $\tilde{\mathbf{d}}_k = \mathbf{g}_1$ and the coefficient vector $\tilde{\mathbf{x}}_T^k = \Delta[1,1] \cdot \mathbf{v}_1$, where, $\mathbf{g}_1$ and $\mathbf{v}_1$ are the first column of $\mathbf{G}$ and $\mathbf{V}$, respectively.
End

Update: $J = J + 1$.

In the MCA-SAR method, the DCT dictionary is used to initialize the clutter dictionary, and the clutter separated by the MCA method is employed as training samples of the K-SVD algorithm. For different scenes, the separated clutter component corresponds to their respective backgrounds, making the resultant clutter dictionary more adaptable.

Considering that most targets have edge or linear features, and strong point targets are easy to be detected, the target dictionary can be focused on linear features. Therefore, the curvelet transform, which can capture edge and linear information accurately and has lower computational complexity than the K-SVD algorithm, is used as the target dictionary here.

3) SAR Echo Sparse Decomposition: For the SAR echo decomposition, a two-step process is employed, including the MCA separation stage and the dictionary update stage. Let the target component and clutter component be $\boldsymbol{s}_t$ and $\boldsymbol{s}_c$ respectively, and use the SAR echo as the initial value, i.e. $\boldsymbol{s}_t = \boldsymbol{s}_c = \boldsymbol{s}$. Set the number of MCA iterations as N_{iter} and the number of dictionary training times as L_{max}.

Step 1. MCA separation

The MCA method is applied to sparsely decompose the SAR echo into target signal, clutter signal and noise, by using a successive iteration method with a varying threshold to find each component [21].

Since the MCA is an iterative coarse-to-fine process, the main information of each component can be extracted at each iteration by the threshold [41]. The threshold linearly decreases to the minimum during iteration.

For the kth MCA iteration, the threshold λ_k is set as [42]:

$$\lambda_k = \lambda_1 - (k-1)\frac{(\lambda_1 - \lambda_{min})}{(N_{iter}-1)} \quad 1 \le k \le N_{iter} \tag{24}$$

where, λ_1 denotes the initial threshold and can be set to a large enough value $\lambda_1 = \min\{\|\boldsymbol{\Phi}_t^+ \mathbf{Ms}\|_\infty, \|\boldsymbol{\Phi}_c^+ \mathbf{Ms}\|_\infty\}$, and λ_{min} is the stopping threshold.

Target separation: Keep the clutter component fixed, using the OMP algorithm [26] to calculate the sparse coefficients $\boldsymbol{\alpha}_t = \boldsymbol{\Phi}_t^+ \mathbf{Ms}_t$. Since the sparse coefficients of the target component is larger than the other components in the target dictionary, the hard thresholding method is used to process the coefficients: $\boldsymbol{\alpha}_t^* = \delta_{\lambda_k}(\boldsymbol{\alpha}_t)$, where $\boldsymbol{\alpha}_t^*$ represents the sparse coefficients larger than the threshold. In the hard thresholding process [43], if $|u| > \lambda$, $\delta_\lambda(u) = u$; otherwise, $\delta_\lambda(u) = 0$.

Reconstruct the target component: $\mathbf{T} = \mathbf{H}\boldsymbol{\Phi}_t \boldsymbol{\alpha}_t^*$.

Clutter separation: Keep the target component fixed, use the OMP algorithm to calculate the sparse coefficients of clutter signal: $\boldsymbol{\alpha}_c = \boldsymbol{\Phi}_c^+ \mathbf{Ms}_c$, update clutter coefficients by hard thresholding: $\boldsymbol{\alpha}_c^* = \delta_{\lambda_k}(\boldsymbol{\alpha}_c)$, and then reconstruct the clutter component: $\mathbf{C} = \mathbf{H}\boldsymbol{\Phi}_c \boldsymbol{\alpha}_c^*$.

After separation, compute the residuals $\mathbf{R} = \mathbf{s} - \mathbf{T} - \mathbf{C}$. In addition to noise, the residuals are likely to contain salient information of clutter or target components. By alternating the process for different components, the estimates of $\mathbf{T}$ and $\mathbf{C}$ are progressively refined.

So, if $k \le N_{iter}$, calculate the threshold λ_k, update $\mathbf{s}_t = \mathbf{T} + \mathbf{R}$, $\mathbf{s}_c = \mathbf{C} + \mathbf{R}$, and return to "Target separation" and continue.

Otherwise, output the separated clutter signal $\mathbf{C}$ and target signal $\mathbf{T}$, and perform Step 2.

Step 2. Clutter dictionary update

Considering the complexity of background clutter and the adaptability of clutter dictionary, after recovering the target signal $\mathbf{T}$ and clutter signal $\mathbf{C}$, the K-SVD dictionary training algorithm is applied to update the clutter dictionary according to the newly recovered clutter component.

When the clutter dictionary is updated, return to Step 1, using the updated clutter dictionary to perform MCA separation on the SAR echo.

Since the target signal tends to reach a stable value after a finite number of clutter dictionary updates, the reconstructed target signal error $\Delta\mathbf{T}$ is used as an iteration stop condition for clutter dictionary updates. For the w th dictionary training iteration, the stopping criterion is

$$\Delta\mathbf{T} = \|\mathbf{T}_w\|_2^2 - \|\mathbf{T}_{w-1}\|_2^2 \le \delta \tag{25}$$

where δ denotes the termination threshold.

Dictionary update is performed until the number of iterations reaches the maximum number L_{max} or the target signal error is below the termination threshold δ.

4) SAR imaging of target component: The spatial geometric relationship between the radar and the observation target remains unchanged after the MCA separation process, so any existing imaging algorithm can be applied to the final recovered target signal. As an example, here the RDA in [7] is used to perform SAR imaging.

IV. Experimental Results

In this section, experimental results based on simulated and real SAR echo data are provided to demonstrate the performance of the proposed method. Traditional RDA [7] and approximate observation-based CS-SAR [19] are employed as imaging methods to compare with the proposed one. The CS-SAR method is solved by ITA, and its specific principle and implementation can be found in [19]. Since clutter suppression in SAR images can be achieved by adaptive spatial-domain filters [44], the widely used Lee [45] and Frost filters [46] are employed to filter the image generated by RDA.

To show the importance of dictionary selection in the proposed MCA-SAR method in an intuitive way, two pairs of dictionaries are introduced. One is to use the DCT dictionary for the clutter and the curvelet dictionary for the target, denoted as MCA-SAR-DCT. The other is to use the K-SVD dictionary training algorithm to construct the clutter dictionary, while using the curvelet dictionary for the target, denoted as MCA-SAR-KSVD. Two commonly used performance indexes, signal-to-clutter ratio (SCR) and the background suppression factor (BSF) are adopted for quantitatively evaluating the performance of all SAR images.

A. Results with Simulated Data

The SAR echo is simulated for two observed scenes: the sea surface with ship wake and the grassland parked with several vehicles. The main parameters are listed in Table II. After determining the scene scattering coefficient based on an

existing real SAR image, the side-looking strip map SAR echo signal is generated with the method in [47]. The RDA, CS-SAR, MCA-SAR-DCT, and MCA-SAR-KSVD are used to image the SAR methods are selected empirically [48]. In the sea surface scene, the free parameters of the MCA-SAR-DCT method are set as follows: the number of MCA iterations N_{iter} =4, the stop threshold λ_{min} =20, and the total number of scale layers for the curvelet transform γ =8; for the MCA-SAR-KSVD method, the K-SVD dictionary training iteration number L_{max} =10, and the other parameters are consistent with those in MCA-SAR-DCT. The free parameters of the grassland scene are set as N_{iter} =4, λ_{min} =2, γ =8 in the MCA-SAR-DCT method, and L_{max} =10 for the MCA-SAR-KSVD method. The imaging results for the two scenes are shown in Fig. 2(a), (b), (e), (f) and Fig. 3(a), (b), (e), (f), respectively. The Lee and Frost filters are used to process the RDA imaging result shown in Fig. 2(a) and Fig. 3(a), and the filtering results are shown in Fig. 2(c)-(d) and Fig. 3(c)-(d).

TABLE II
PARAMETERS OF SAR SYSTEM

Pulse repetition frequency	500HZ	Slant range of scene center	14.6km
Pulse duration	2μs	Velocity	200m/s
Center frequency	10GHZ	Sampling Rate	240MHz
Range FM rate	100MHz/μs	Beam squint angle	0 rad

It can be seen from Fig. 2 that all SAR images can show the main structure of ship wakes. However, there is a lot of clutter on the sea surface of Fig. 2(a). The clutter is relatively strong which will affect the detection of ship wakes. In Fig. 2(b), the clutter is still not suppressed enough, and some details of ship wakes are buried. For the filtered results in Fig. 2(c) and Fig. 2(d), the SAR image pixels are averaged, and in low-contrast or edge areas, the distinction at the boundary between the target and clutter is not clear. In the MCA-SAR results shown in Fig. 2(e) and Fig. 2(f), the clutter and noise of sea surface are significantly suppressed, and the ship wakes can be seen more clearly.

By comparing Fig. 2(e) with Fig. 2(f), it can be found that the ship wakes of MCA-SAR-KSVD are clearer than those of MCA-SAR-DCT, because the K-SVD algorithm adopted in MCA-SAR-KSVD can help find a more suitable clutter dictionary, which can sparsely represent the clutter better than the fixed DCT dictionary in MCA-SAR-DCT.

Fig. 3 shows the results of grassland. For the RDA result in Fig. 3(a), the clutter is so strong that the SAR image is rough. In Fig. 3(b), most of the background clutter still exists in the image produced by CS-SAR, which affects the small paths. In Fig. 3(c) and Fig. 3(d), it can be observed that the Lee and Frost filters can effectively filter out the background clutter, but they are not able to preserve those delicate parts of the target, such as the edge of the point target and roads.

In Fig. 3(e) and Fig. 3(f), it is shown that the MCA-SAR methods can effectively suppress the clutter and noise, and smooth grassland surface while roads with linear characteristics are enhanced and easier to detect. Although the curvelet dictionary is used to represent the target component in the MCA-SAR methods, the point targets are still obvious in Fig. 3(e) and Fig. 3(f). Comparing the two different clutter dictionaries, MCA-SAR-KSVD achieves a better clutter and noise suppression effect than MCA-SAR-DCT, which means that K-SVD has provided a better clutter dictionary through the adopted iterative training process.

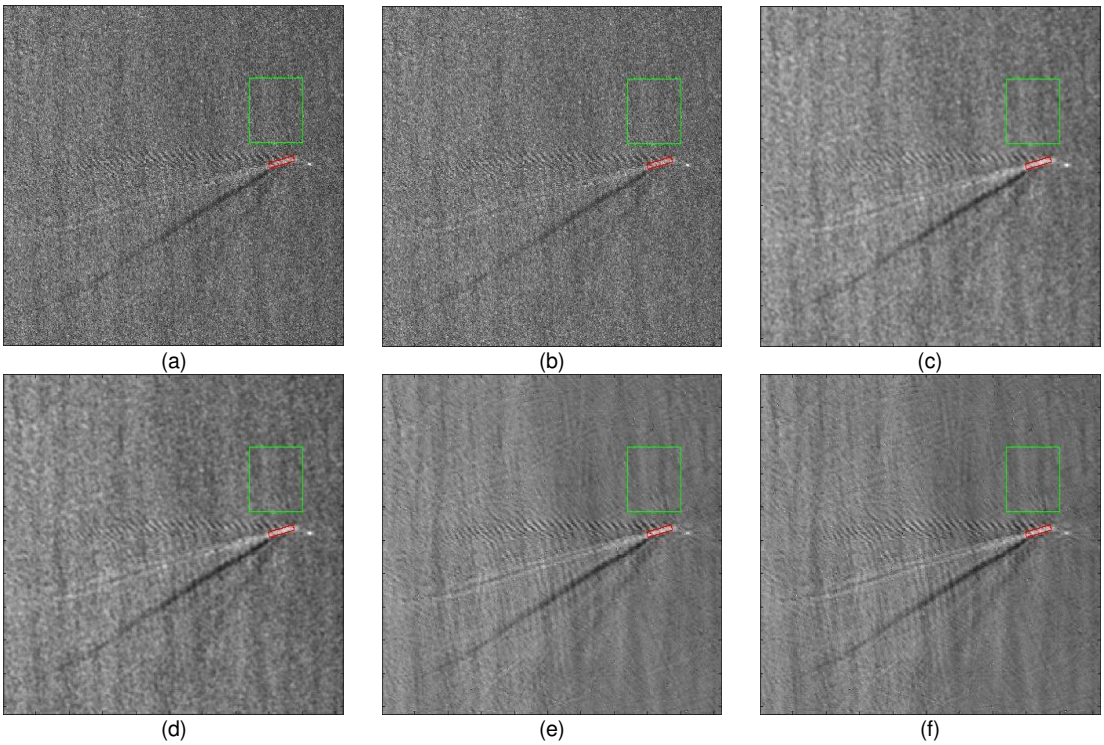

Fig. 2. Imaging results of sea surface. (a) RDA. (b) CS-SAR. (c) RDA + Lee filter. (d) RDA + Frost filter. (e) MCA-SAR-DCT. (f) MCA-SAR-KSVD.

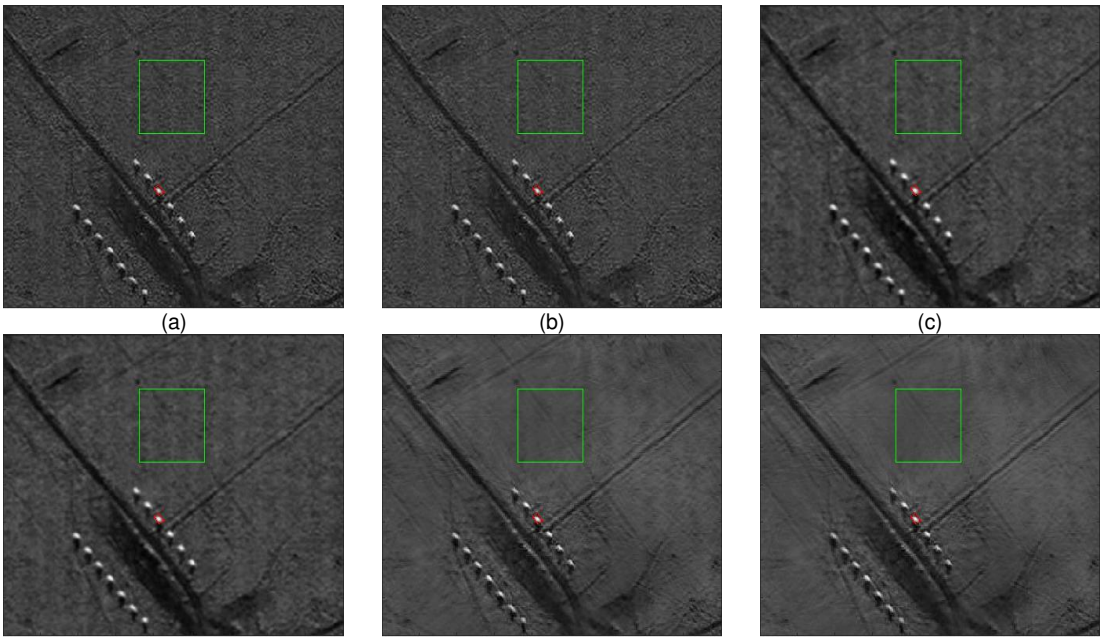

Fig. 3. Imaging results of grassland. (a) RDA. (b) CS-SAR. (c) RDA + Lee filter. (d) RDA + Frost filter. (e) MCA-SAR-DCT. (f) MCA-SAR-KSVD.

To illustrate the clutter and noise suppression performance in a quantitative way, the SCR and BSF are used to evaluate the imaging results, and they are defined as follows [49] [50]:

$$\mathrm{SCR} = 20\log\left(\frac{\mu_t-\mu_c}{\sigma_c}\right) \tag{26}$$

$$\mathrm{BSF} = \frac{\sigma_{in}}{\sigma_c} \tag{27}$$

where, μ_t and μ_c denote the average gray value of the target and non-target areas, respectively, σ_c is the standard deviation of gray values in non-target areas, and σ_{in} represents that of the non-target areas in the image obtained by RDA. As it is difficult to distinguish noise from the background clutter, the suppression ability for clutter and noise is evaluated together. The target and non-target areas are marked by the red and green rectangles respectively in the images of each scene. The results are shown in Table III.

In Table III, the SCR values of RDA for the sea surface and grassland are 4.23 dB and 13.41 dB, respectively, while for CS-SAR, they are 4.24 dB and 13.88 dB, a little better than RDA. The difference of SCR between the Lee and Frost filters in the two scenes is very small, and they are 13.49 dB and 13.45 dB, 17.63 dB and 17.72 dB, respectively. For MCA-SAR-DCT, the SCR values in the two scenes are 13.83 dB and 18.61 dB, respectively. For the MCA-SAR-KSVD method, they are 14.31 dB and 20.04 dB respectively. Comparing the SCR values of different methods, it can be seen that the SCR value of MCA-SAR-KSVD is the highest. Although Lee and Frost filters can achieve effective clutter suppression and obtain better evaluation results, it can be seen from Fig. 2(c), (d) and Fig. 3(c), (d) that they also blur the target, so a visually degraded target is presented.

Table III also shows that, in the image reconstructed by CS-SAR, the BSF value is usually very low. The MCA-SAR methods can improve BSF more significantly than the other methods, and the BSF of MCA-SAR-KSVD is better than MCA-SAR-DCT. The results of both SCR and BSF show that the proposed MCA-SAR methods can reduce the effect of clutter and noise significantly, and the performance of MCA-SAR-KSVD is better than MCA-SAR-DCT. The main advantage of the MCA-SAR-KSVD method is that it can operate properly in an unknown clutter environment since it does not require prior information before imaging and can perform dictionary learning based on the clutter separated by the MCA method.

TABLE III
SCR, BSF, AND RUNNING TIME OF SIMULATED RESULTS

Methods	Sea scene			Grassland scene		
	SCR (dB)	BSF	Running time (s)	SCR (dB)	BSF	Running time (s)
RDA	4.23	1.00	0.13	13.41	1.00	0.11
CS-SAR	4.24	1.03	0.61	13.88	1.05	1.04
Lee filter	13.49	1.89	8.81	17.63	1.24	6.18
Frost filter	13.45	1.80	7.31	17.72	1.26	5.15
MCA-SAR-DCT	13.83	2.33	51.43	18.61	2.06	70.23

MCA-SAR-KSVD	**14.31**	**2.50**	**211.37**	**20.04**	**2.27**	**282.01**

A computer with an Intel CPU E5-2680 processor and 192GB main memory is used in the experiments. The running time of the five methods is also listed in Table III. It is shown that the MCA-SAR methods take more time than the other methods because the MCA-SAR methods require dictionary construction and sparse representation in the MCA iterative process, which is more complex and time-consuming. The MCA-SAR-KSVD method exhibits a significant increase in running time over the MCA-SAR-DCT method because it uses an iterative process for dictionary update and the K-SVD dictionary training algorithm requires a large amount of computation.

B. Real Data Experiment

The experiment data was collected by RADARSAT-1 in Vancouver on June 16, 2002 [7]. The RDA, CS-SAR, and the proposed MCA-SAR methods are used to process the RADARSAT-1 echo data. The Lee and Frost filters are applied to suppress clutter in the images obtained by the RDA. Two scenes are selected: the sea surface with strong clutter and the ground with a large amount of clutter. Table IV lists the primary SAR parameters of RADARSAT-1.

TABLE IV
PARAMETERS OF RADARSAT-1

Pulse repetition frequency	1256.98HZ	Slant range of scene center	1016.7km
Pulse duration	41.74μs	Velocity	7062m/s
Center frequency	5.30GHZ	Sampling Rate	32.317MHz
Range FM rate	0.72MHz/μs	Beam squint angle	0.06 rad

The imaging results of the sea surface are shown in Fig. 4 and those of the ground scene are shown in Fig. 5. For the MCA-SAR-DCT method, the free parameters of the two scenes are set as N_{iter} =8, λ_{min} =22, $\gamma = 8$ and $N_{iter} = 5$, λ_{min} =2, γ =4, respectively. For the MCA-SAR-KSVD method, the additional K-SVD dictionary training parameter for the two scenes is L_{max} =8.

Fig. 4(a) is the imaging result by the RDA method, Fig. 4(b) is the reconstruction result of the CS-SAR method. Fig. 4(c) and Fig. 4(d) are the filtering results of Lee and Frost filters for Fig. 4(a). Fig. 4(e) and Fig. 4(f) are the results of the proposed MCA-SAR methods, with Fig. 4(e) for the MCA-SAR-DCT method and Fig. 4(f) for the MCA-SAR-KSVD method. In Fig. 4(a), it can be seen that the imaging result of RDA is extremely noisy, with a lot of clutter. In Fig. 4(b), the clutter suppression effect of the CS-SAR method is modest and some clutter is preserved to a certain extent. The resultant filtered images of Fig. 4(c) and Fig. 4(d) are milder than the original image, but at a cost of degraded target discrimination. From Fig. 4(e) and Fig. 4(f), results of MCA-SAR methods, it can be seen that the linear target is reconstructed well from the curvelet dictionary, and sea clutter and noise have been better suppressed than the other methods. The choice of clutter dictionary affects the result of clutter suppression to a degree. By comparing Fig. 4(e) and Fig. 4(f), the SAR image of MCA-SAR-KSVD contains less background clutter visually than that of MCA-SAR-DCT.

To examine the results in more detail, the enlarged results for the white rectangular area in Fig. 4 are shown in Fig. 6 for the six considered methods. As can be seen, the target is surrounded by strong clutter in the RDA result and some clutter remains in the image obtained by CS-SAR; the Lee and Frost filters can

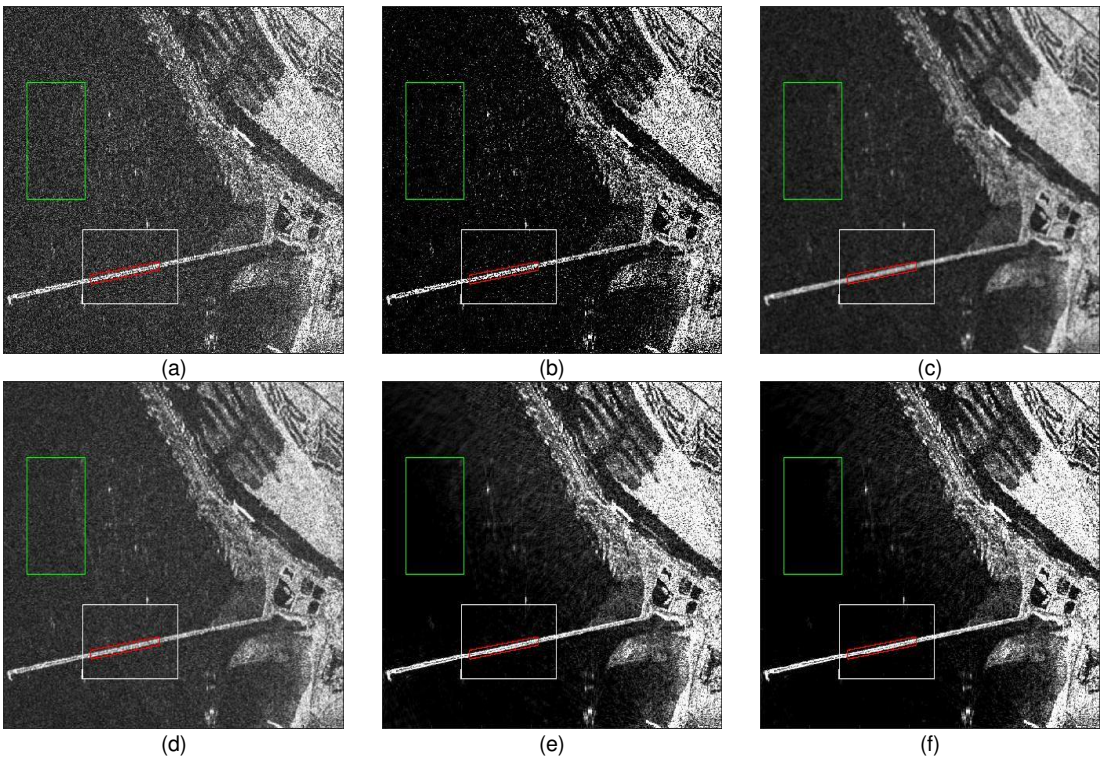

Fig. 4. RADARSAT-1 imaging results of the sea surface. (a) RDA. (b) CS-SAR. (c) RDA + Lee filter. (d) RDA + Frost filter. (e) MCA-SAR-DCT.

(f) MCA-SAR-KSVD.

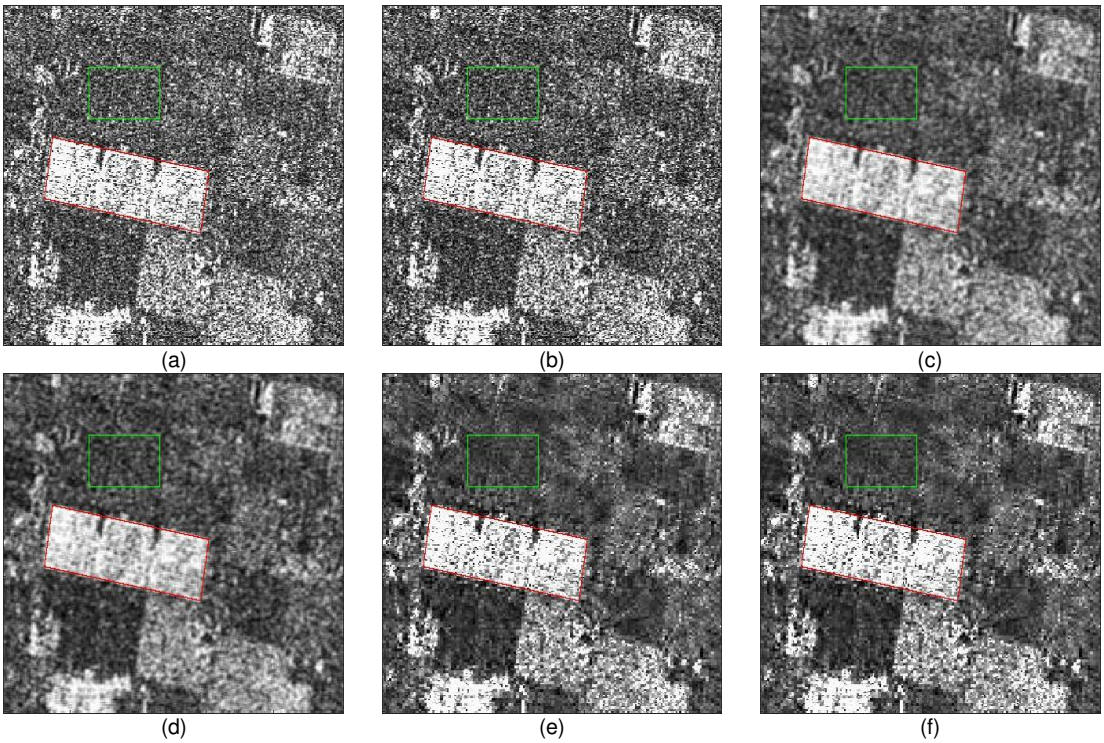

Fig. 5. RADARSAT-1 imaging results of the ground. (a) RDA. (b) CS-SAR. (c) RDA + Lee filter. (d) RDA + Frost filter. (e) MCA-SAR-DCT. (f) MCA-SAR-KSVD.

smooth the image sufficiently, but they also reduce the sharpness of the target region; in contrast, the two MCA-SAR methods can give a much clearer result, highlighting the linear contour features of the target area and suppressing noise and clutter.

The MCA-SAR methods using the curvelet transform as the target dictionary can also enhance the point target, but the enhancement is less than the linear target. For example, it is difficult to visually capture the two ships in the lower-left corner of Fig. 4 in the MCA-SAR results. Although the intensity of the point target is increased relative to the surrounding clutter, image quantization causes visual attenuation of the ship targets due to stronger enhancement of the linear target (bridge).

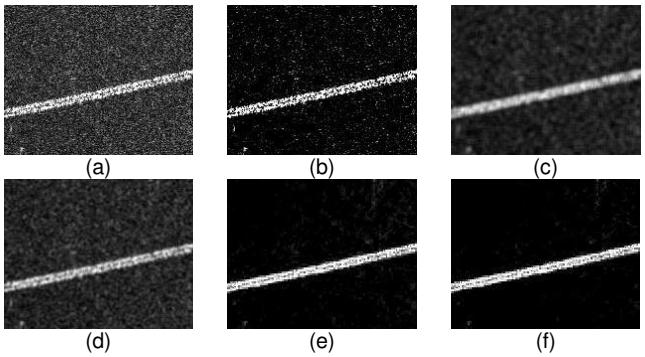

Fig. 6. Detailed comparison on the selected area at an enlarged scale. (a) RDA. (b) CS-SAR. (c) RDA + Lee filter. (d) RDA + Frost filter. (e) MCA-SAR-DCT. (f) MCA-SAR-KSVD.

Fig. 5(a) shows the RDA imaging result of the ground region which is composed of a target and strong clutter. For the CS-SAR result in Fig. 5(b), there is still obvious clutter in the background, and the contrast between the target and clutter is barely increased. In Fig. 5(c) and Fig. 5(d), the Lee and Frost filters have reduced the background clutter effectively, but the edges and fine details are also blurred compared to the original one. In Fig. 5(e) and Fig. 5(f), the MCA-SAR methods have produced a stronger target than the other competing methods, making the distinction between the target area and other areas more clearly by enhancing the target region while removing the clutter and noise. Although the clutter suppression effect of the MCA-SAR-KSVD method is visually almost indistinguishable from that of MCA-SAR-DCT, the evaluation indicators SCR and BSF can prove the superior performance of the MCA-SAR-KSVD method. The high-quality imaging results by the MCA-SAR-KSVD method benefit from the iterative decomposition of SAR echoes and the update of clutter dictionary, at a cost of reduced efficiency, as shown in Table V.

The SCR and BSF values of all methods are also presented in Table V. It can be seen that both MCA-SAR methods have achieved better results than the others, e.g., for the sea surface, the SCR value of the MCA-SAR methods is at least 5.45 dB larger than those of other methods, and the BSF value of the MCA-SAR methods is at least 0.27 larger. It indicates that the MCA-SAR methods can effectively distinguish useful target components from clutter and noise, increase the contrast between the target and the clutter, and significantly suppress the clutter and noise.

For the ground scene, the SCR and BSF values of MCA-SAR-DCT and MCA-SAR-KSVD are 17.47 dB and 2.45, 17.59

dB and 2.49, respectively, which are higher than the other methods. But compared with the sea surface case, the value of both MCA-SAR methods is relatively close. This is consistent with the fact that the target in the ground scene cannot be completely expressed by linear features so that it is difficult to fully detect the target using the curvelet dictionary, and the pertinence of the dictionary learning is weakened. In addition, when the observed scene contains various types of clutter simultaneously, the sparse representation competence of the learned clutter dictionary will inevitably decrease, so the clutter cannot be completely separated from the SAR echo, which will affect the clutter suppression ability of the proposed method to a certain extent.

But overall, a similar conclusion can be drawn as in the simulated data, i.e., the proposed MCA-SAR methods are superior to the other considered methods in the imaging results. Among all the methods, MCA-SAR-KSVD provides the best result, which indicates that applying the K-SVD dictionary training algorithm to construct the clutter dictionary can better represent the clutter and then suppress it in the following MCA operation. Consequently, the resultant image by MCA-SAR-KSVD has a high target and clutter contrast and fine details.

TABLE V
SCR, BSF, AND RUNNING TIME OF REAL DATA RESULTS

Methods	Sea scene			Ground scene		
	SCR (dB)	BSF	Running time (s)	SCR (dB)	BSF	Running time (s)
RDA	6.59	1.00	0.21	7.67	1.00	0.04
CS-SAR	13.28	1.31	0.98	7.81	0.99	0.28
Lee filter	18.76	3.78	14.85	16.03	2.41	2.18
Frost filter	14.84	2.54	12.88	16.02	2.34	1.91
MCA-SAR-DCT	24.21	4.05	1865.64	17.47	2.45	20.44
MCA-SAR-KSVD	**27.05**	**5.15**	**13152.38**	**17.59**	**2.49**	**354.03**

V. CONCLUSION

A novel SAR imaging method based on MCA has been proposed for effective clutter suppression. The SAR echo is modeled as a linear combination of the target signal, clutter signal, and noise. By sparsely representing the target and clutter with different dictionaries, the MCA method is used to decompose the overall SAR echo into three parts corresponding to target signal, clutter signal, and noise, respectively; to suppress clutter and noise, only the separated target signal is processed to give the final imaging result. Two different ways to construct the clutter dictionary were provided: one is based on a fixed dictionary, and one is adaptive and learned through the recovered clutter in an iterative way using the K-SVD algorithm. As demonstrated by results based on both simulated and real data, the proposed MCA-SAR method can suppress clutter and noise effectively, while as expected the one based on adaptive dictionary has provided the best result. As a fine imaging method with a high computational complexity, when the proposed MCA-SAR method is applied to large-scale SAR imaging, its adaptive parallel block processing needs to be investigated in the future work.

REFERENCES

[1] K. Radecki, P. Samczyński and D. Gromek, "Fast Barycentric-Based Back Projection Algorithm for SAR Imaging," in IEEE Sensors Journal, vol. 19, no. 22, pp. 10635-10643, 15 Nov.15, 2019, doi: 10.1109/JSEN.2019.2932200.

[2] Mahafza B. R. Radar Systems Analysis and Design Using MATLAB, 3e. CRC Press, Inc.

[3] M. Shi, L. Ling, J. Li and L. Wang, "Infrared background clutter analysis and the quantitative method research," 2017 9th International Conference on Advanced Infocomm Technology (ICAIT), 2017, pp. 297-299, doi: 10.1109/ICAIT.2017.8388933.

[4] J. A. Ratches, C. P. Walters, R. G. Buser and B. D. Guenther, "Aided and automatic target recognition based upon sensory inputs from image forming systems," in IEEE Transactions on Pattern Analysis and Machine Intelligence, vol. 19, no. 9, pp. 1004-1019, Sept. 1997.

[5] S. Jinping, Y. Zhenyu, H. Kunxi and H. Yuxin, "High resolution SAR imaging of ground moving target in dense clutter environments," 2015 IEEE 5th Asia-Pacific Conference on Synthetic Aperture Radar (APSAR), 2015, pp. 400-404.

[6] Y. Yang, Y. Pi and R. Li, "Back Projection Algorithm for Spotlight Bistatic SAR Imaging," 2006 CIE International Conference on Radar, 2006, pp. 1-4.

[7] Ian G. Cumming, Frank H. Wong, "Digital processing of synthetic aperture radar data, algorithm and implementation", Artech House, 2005.

[8] R. K. Raney, H. Runge, R. Bamler, I. G. Cumming and F. H. Wong, "Precision SAR processing using chirp scaling," in IEEE Transactions on Geoscience and Remote Sensing, vol. 32, no. 4, pp. 786-799, July 1994.

[9] W. G. Carrara, R. S. Goodman and R. M. Majewski, "Spotlight synthetic aperture radar signal processing algorithms", Artech House, Boston, 1995.

[10] X. Quan, Z. Zhang, B. Zhang, W. Hong and Y. Wu, "A study of BP-camp algorithm for SAR imaging," 2015 IEEE International Geoscience and Remote Sensing Symposium (IGARSS), 2015, pp. 4480-4483.

[11] C. Oliver and S. Quegan, "Understanding Synthetic Aperture Radar Images", Norwood, MA: Artech House, 1998.

[12] S. R. DeGraaf, "SAR imaging via spectral estimation methods," Proceedings of 1994 28th Asilomar Conference on Signals, Systems and Computers, 1994, pp. 117-121 vol.1.

[13] V. M. Patel, G. R. Easley, D. M. Healy and R. Chellappa, "Compressed Synthetic Aperture Radar," in IEEE Journal of Selected Topics in Signal Processing, vol. 4, no. 2, pp. 244-254, April 2010.

[14] R. Schmidt, "Multiple emitter location and signal parameter estimation," in IEEE Transactions on Antennas and Propagation, vol. 34, no. 3, pp. 276-280, March 1986.

[15] H. Jiang, B. Zhang, Y. Lin, W. Hong, Y. Wu and J. Zhan, "Random noise SAR based on compressed sensing," 2010 IEEE International Geoscience and Remote Sensing Symposium, 2010, pp. 4624-4627.

[16] M. Kang and K. Kim, "Compressive Sensing Based SAR Imaging and Autofocus Using Improved Tikhonov Regularization," in IEEE Sensors Journal, vol. 19, no. 14, pp. 5529-5540, 15 July15, 2019, doi: 10.1109/JSEN.2019.2904611.

[17] M. Tello Alonso, P. Lopez-Dekker and J. J. Mallorqui, "A Novel Strategy for Radar Imaging Based on Compressive Sensing," in IEEE Transactions

on Geoscience and Remote Sensing, vol. 48, no. 12, pp. 4285-4295, Dec. 2010.
[18] H. Jiang, ChengLong Jiang, B. Zhang, W. Hong and Y. Wu, "Experimental results of spaceborne stripmap SAR raw data imaging via compressed sensing," Proceedings of 2011 IEEE CIE International Conference on Radar, 2011, pp. 202-205.
[19] J. Fang, Z. Xu, B. Zhang, W. Hong and Y. Wu, "Fast Compressed Sensing SAR Imaging Based on Approximated Observation," in IEEE Journal of Selected Topics in Applied Earth Observations and Remote Sensing, vol. 7, no. 1, pp. 352-363, Jan. 2014.
[20] Turek J S, Elad M, Yavneh I. Clutter Mitigation in Echocardiography Using Sparse Signal Separation[J]. International Journal of Biomedical Imaging, 2015, 2015:1-18.
[21] Temlioglu E, Erer I. Clutter Removal in Ground-Penetrating Radar Images Using Morphological Component Analysis[J]. IEEE Geoscience and Remote Sensing Letters, 2016:1802-1806.
[22] J. Ni, Q. Zhang, Y. Luo and L. Sun, "Compressed Sensing SAR Imaging Based on Centralized Sparse Representation," in IEEE Sensors Journal, vol. 18, no. 12, pp. 4920-4932, 15 June15, 2018.
[23] Mallat and Z. Zhang, "Matching pursuits with time–frequency dictionaries," IEEE Trans. Signal Process., vol. 41, no. 12, pp. 3397–3415, Dec. 1993.
[24] J. -. Starck, M. Elad and D. L. Donoho, "Image decomposition via the combination of sparse representations and a variational approach," in IEEE Transactions on Image Processing, vol. 14, no. 10, pp. 1570-1582, Oct. 2005.
[25] J. M. Bioucas-Dias and M. A. T. Figueiredo, "A new TwIST: Two-step iterative shrinkage/thresholding algorithms for image restoration," IEEE Trans. Image Process., vol. 16, no. 12, pp. 2992–3007, Dec. 2007.
[26] J. Tropp and A. Gilbert, "Signal recovery from random measurements via orthogonal matching pursuit," IEEE Trans. Inf. Theory, vol. 53, no. 12,pp. 4655–4666, Dec. 2007.
[27] Budianto, D. P. K. Lun and Y. Chan, "Robust Single-Shot Fringe Projection Profilometry Based on Morphological Component Analysis," in IEEE Transactions on Image Processing, vol. 27, no. 11, pp. 5393-5405, Nov. 2018.
[28] J. -. Starck, M. Elad and D. L. Donoho, "Image decomposition via the combination of sparse representations and a variational approach," in IEEE Transactions on Image Processing, vol. 14, no. 10, pp. 1570-1582, Oct. 2005
[29] I. Daubechies, "The wavelet transform, time-frequency localization and signal analysis," in IEEE Transactions on Information Theory, vol. 36, no. 5, pp. 961-1005, Sept. 1990.
[30] Jean-Luc Starck, E. J. Candes and D. L. Donoho, "The curvelet transform for image denoising," in IEEE Transactions on Image Processing, vol. 11, no. 6, pp. 670-684, June 2002.
[31] A. Qayyum et al., "Designing of overcomplete dictionaries based on DCT and DWT," 2015 IEEE Student Symposium in Biomedical Engineering & Sciences (ISSBES), 2015, pp. 134-139.
[32] F. Giovanneschi, K. V. Mishra, M. A. Gonzalez-Huici, Y. C. Eldar and J. H. G. Ender, "Online dictionary learning aided target recognition in cognitive GPR," 2017 IEEE International Geoscience and Remote Sensing Symposium (IGARSS), 2017, pp. 4813-4816, doi: 10.1109/IGARSS.2017.8128079.
[33] K. Engan, S. O. Aase and J. Hakon Husoy, "Method of optimal directions for frame design," 1999 IEEE International Conference on Acoustics, Speech, and Signal Processing. Proceedings. ICASSP99 (Cat. No.99CH36258), 1999, pp. 2443-2446 vol.5.
[34] Mairal J , Bach F , Ponce J , et al. Online dictionary learning for sparse coding[C]// International Conference on Machine Learning. DBLP, 2009.
[35] M. Aharon, M. Elad and A. Bruckstein, "K-SVD: An algorithm for designing overcomplete dictionaries for sparse representation," in IEEE Transactions on Signal Processing, vol. 54, no. 11, pp. 4311-4322, Nov. 2006.
[36] J. Chi and M. Eramian, "Enhancement of Textural Differences Based on Morphological Component Analysis," in IEEE Transactions on Image Processing, vol. 24, no. 9, pp. 2671-2684, Sept. 2015.
[37] X. Qiao, T. Shan, R. Tao, X. Bai and J. Zhao, "Separation of Human Micro-Doppler Signals Based on Short-Time Fractional Fourier Transform," in IEEE Sensors Journal, vol. 19, no. 24, pp. 12205-12216, 15 Dec.15, 2019, doi: 10.1109/JSEN.2019.2937989.
[38] H. Van Nguyen, V. M. Patel, N. M. Nasrabadi and R. Chellappa, "Design of Non-Linear Kernel Dictionaries for Object Recognition," in IEEE Transactions on Image Processing, vol. 22, no. 12, pp. 5123-5135, Dec. 2013, doi: 10.1109/TIP.2013.2282078.
[39] X. Zhan, R. Zhang, D. Yin and C. Huo, "SAR Image Compression Using Multiscale Dictionary Learning and Sparse Representation," in IEEE Geoscience and Remote Sensing Letters, vol. 10, no. 5, pp. 1090-1094, Sept. 2013, doi: 10.1109/LGRS.2012.2230394.
[40] I. Kviatkovsky, M. Gabel, E. Rivlin and I. Shimshoni, "On the Equivalence of the LC-KSVD and the D-KSVD Algorithms," in IEEE Transactions on Pattern Analysis and Machine Intelligence, vol. 39, no. 2, pp. 411-416, 1 Feb. 2017.
[41] M. J. Fadili, J. Starck, J. Bobin and Y. Moudden, "Image Decomposition and Separation Using Sparse Representations: An Overview," in Proceedings of the IEEE, vol. 98, no. 6, pp. 983-994, June 2010.
[42] J. Bobin, J. Starck, J. M. Fadili, Y. Moudden and D. L. Donoho, "Morphological Component Analysis: An Adaptive Thresholding Strategy," in IEEE Transactions on Image Processing, vol. 16, no. 11, pp. 2675-2681, Nov. 2007.
[43] C. Yu, Q. Qiu, Y. Zhao and X. Chen, "Satellite Image Classification Using Morphological Component Analysis of Texture and Cartoon Layers," in IEEE Geoscience and Remote Sensing Letters, vol. 10, no. 5, pp. 1109-1113, Sept. 2013.
[44] X. Zhao, Y. Jiang and W. Wang, "Efficient Clutter Suppression in SAR Images with Shedding Irrelevant Patterns," in IEEE Geoscience and Remote Sensing Letters, vol. 12, no. 9, pp. 1828-1832, Sept. 2015, doi: 10.1109/LGRS.2015.2430366.
[45] J. -S. Lee, "Digital Image Enhancement and Noise Filtering by Use of Local Statistics," in IEEE Transactions on Pattern Analysis and Machine Intelligence, vol. PAMI-2, no. 2, pp. 165-168, March 1980, doi: 10.1109/TPAMI.1980.4766994.
[46] V. S. Frost, J. A. Stiles, K. S. Shanmugan and J. C. Holtzman, "A Model for Radar Images and Its Application to Adaptive Digital Filtering of Multiplicative Noise," in IEEE Transactions on Pattern Analysis and Machine Intelligence, vol. PAMI-4, no. 2, pp. 157-166, March 1982, doi: 10.1109/TPAMI.1982.4767223.
[47] Y. Shen, X. Wang, H. Chen and X. Hao, "SAR raw echo simulation of ground scene," 2010 3rd International Congress on Image and Signal Processing, 2010, pp. 2251-2254.
[48] X. Xu, J. Li, X. Huang, M. Dalla Mura and A. Plaza, "Multiple Morphological Component Analysis Based Decomposition for Remote Sensing Image Classification," in IEEE Transactions on Geoscience and Remote Sensing, vol. 54, no. 5, pp. 3083-3102, May 2016, doi: 10.1109/TGRS.2015.2511197.
[49] H. Deng, X. Sun, M. Liu, C. Ye and X. Zhou, "Small Infrared Target Detection Based on Weighted Local Difference Measure," in IEEE Transactions on Geoscience and Remote Sensing, vol. 54, no. 7, pp. 4204-4214, July 2016.
[50] J. Han, Y. Ma, J. Huang, X. Mei and J. Ma, "An Infrared Small Target Detecting Algorithm Based on Human Visual System," in IEEE Geoscience and Remote Sensing Letters, vol. 13, no. 3, pp. 452-456, March 2016, doi: 10.1109/LGRS.2016.2519144.